Separation and Purification Technology 177 (2017) 272–280

Contents lists available at ScienceDirect

Separation and Purification Technology

journal homepage: www.elsevier.com/locate/seppur

Adsorption of three selected pharmaceuticals and personal care products (PPCPs) onto MIL-101(Cr)/natural polymer composite beads

Ning Zhuo, Yaqian Lan, Weiben Yang *, Zhen Yang *, Xiaomin Li, Xia Zhou, Yang Liu, Jiachun Shen, Xuntong Zhang

School of Chemistry and Materials Science, Jiangsu Provincial Key Laboratory of Material Cycling and Pollution Control, Nanjing Normal University, Nanjing 210023, PR China

ARTICLE INFO

Article history:
Received 7 June 2016
Received in revised form 15 December 2016
Accepted 26 December 2016
Available online 28 December 2016

Keywords:
Adsorption
PPCPs
MIL-101(Cr)
Composite beads
Electrostatic attraction
π-π interaction

ABSTRACT

Porous metal-organic frameworks (MOFs) have great potential as high-effective adsorbents for water treatment. However, poor separability restricts their practical application. To overcome the drawback, both MIL-101(Cr)/sodium alginate (MIL-101(Cr)/SA) and MIL-101(Cr)/chitosan (MIL-101(Cr)/CS) composite beads were prepared and characterized. Adsorption of three selected pharmaceuticals and personal care products (PPCPs) (benzoic acid (BEN), ibuprofen (IBU) and ketoprofen (KET)) onto the two composite beads was investigated and compared with pristine SA and CS beads. Kinetic plots, pH dependence, isotherm data, and influences of ionic strength were reported. The MIL-101(Cr)/CS beads exhibit much higher adsorption capacity than SA, CS and MIL-101(Cr)/SA, and the adsorption amounts of three PPCPs onto MIL-101(Cr)/CS follow the order of KET > IBU > BEN. The adsorption amounts of the three PPCPs on the MIL-101(Cr)/CS increased quickly during the first 60 min of contact time and then achieved the adsorption equilibrium after ~180 min. Not only the protonated amine groups but also the Cr center of the adsorbents exerted electrostatic attraction with the deprotonated carboxyl groups of contaminants, as elucidated by X-ray photoelectron spectroscopy (XPS). Based on the adsorption isotherms and π-energy analysis of three PPCPs, π-π interaction of aromatic groups between adsorbents and contaminants also contributed to the adsorption. The MIL-101(Cr)/CS beads exhibited good regenerability over several repeated adsorption/desorption cycles. Overall, this study is believed to enlarge the application of MOFs on the removal of emerging contaminants from waters.

1. Introduction

Pharmaceuticals and personal care products (PPCPs) have become important emerging contaminants and attracted much attention due to their possible estrogenic and other adverse effects on humans [1]. PPCPs are introduced not only by humans but also through veterinary use for livestock, poultry, and fish farming, which have been found to be ubiquitous in the aquatic environment [2]. To date, many technologies, such as degradation [3], plant uptake [4], adsorption [5] and so on, have been explored for the removal of PPCPs from aqueous solution.

Compared to other techniques, adsorption is considered as efficient and economical methods for the removal of PPCPs from waters [6,7]. Metal-organic frameworks (MOFs), which are crystalline porous materials constructed from multifunctional ligands and metal ions, have drawn considerable attention for environmental remediation purposes owing to their high porosity and tenability [8,9]. Particularly, most studies concerning adsorption have investigated dyes [10], organoarsenic [11], phenols [12], and heavy metal [13] removal using MOFs nanoparticle from the liquid phase, with the large adsorption capacity and fast adsorption kinetics. However, the use of MOFs nanoparticle is heavily restricted due to their poor separability because significant post-treatment filtration or centrifuge is required to remove the MOFs from the purified water, and obvious loss of adsorbents will happen during such processes. To overcome the shortcoming, immobilization of active micro- or nanoscale particle appears to provide an approach.

Natural polymers have been long favored due to their additional advantages of being inexpensive, plentiful, non-toxic, and renewable [14–16], such as sodium alginate and chitosan, which can be easily formulated into a few millimeters beads easily separated from a liquid medium [17–19]. The flexibility of nanoparticles incorporated into sodium alginate and chitosan are considered to

* Corresponding authors.
E-mail addresses: yangwb007@njnu.edu.cn (W. Yang), yangzhen@njnu.edu.cn (Z. Yang).

http://dx.doi.org/10.1016/j.seppur.2016.12.041
1383-5866/

be an excellent way to immobilize active micro- or nanoscale particles and present novel composite adsorbents. MIL-101(Cr), belonging to a class of chromium(III) terephthalate MOFs, possesses an extremely high specific surface area ($S_{BET} \approx 4000\ m^2/g$), and adsorbate molecules can access its quasi-spherical cages (Ø ≈ 2.9 and 3.4 nm) via 1.2 and 1.6 nm apertures (Supporting Information Fig. S1) [20]. Benefiting from acid and base resistance and aqueous stability, MIL-101(Cr) can be used as a reference MOFs for studying various guest-host interactions for aqueous PPCPs removal. To our best knowledge, removal of PPCPs by MIL-101(Cr)-impregnated sodium alginate or chitosan beads has not been thoroughly studied yet.

In this study, we prepared both novel composite beads of MIL-101(Cr)/SA and MIL-101(Cr)/CS. The adsorption behaviors and mechanisms of three selected PPCPs (benzoic acid (BEN), ibuprofen (IBU) and ketoprofen (KET)) onto the as-synthesized beads were systematically investigated from aqueous media. Pure SA and CS beads were used for comparisons. Adsorption kinetics, effect of pH, adsorption isotherm, and influences of ionic strength were investigated. Desorption and reusability of MIL-101(Cr)/CS were also studied. Finally, the adsorption mechanism was discussed on the basis of the instrumental analysis.

2. Materials and methods

2.1. Materials

Chromic nitrate nonahydrate ($Cr(NO_3)_3{\cdot}9H_2O$, ⩾99%), hydrofluoric acid (HF, ⩾40 wt.%), calcium chloride ($CaCl_2$, ⩾96%), sodium alginate (a viscosity of 0.02Pas in 1% aqueous solution at 20 °C), hydrochloric acid (HCl, 36–38 wt.%), N,N-dimethylformamide (DMF, ⩾99.5%), ethanol (⩾99.7%), benzoic acid (⩾99.5%) and sodium chloride (NaCl, ⩾99.5%) were obtained from the Sinopharm Chemical Reagent Co., Ltd. Terephthalic acid (⩾99%), chitosan (the degree of deacetylation is 95%.), ibuprofen (⩾98%), ketoprofen (⩾98%), glutaraldehyde (⩾50 wt.%) and sodium tripolyphosphate ($Na_5P_3O_{10}$, ⩾98%) were purchased from Aladdin Industrial Corporation. All reagents were used without further treatment. Ultrapure water (18.2 MΩ cm^{-1}) was used in all the experiments.

2.2. Preparation of adsorbents

MIL-101(Cr) nanoparticles were prepared hydro-thermally following the reported methods [20], described in detailed in Supporting Information Text S1. Then, as illustrated in Fig. 1A, a homogeneous aqueous solution of sodium alginate/chitosan (2–3 wt.%) was dropped into a $CaCl_2/Na_5P_3O_{10}$ solution (1–2 wt. %) by using a syringe needle and then 1–3 mm beads were formed through precipitation immediately [17,21].

Subsequently, the beads in the solution were incubated for 30 min (10 h for chitosan) at room temperature. The obtained beads were filtered and rinsed repeatedly by water to remove unreacted Ca^{2+} /$P_3O_{10}^{5+}$ on the surface of the beads. After filtration and rinsing repeatedly, the precipitation cross-linking beads were obtained by suspending in the reaction medium containing 1.58 M glutaraldehyde and 0.38 M HCl at 40 °C for 24 h (0.02 M glutaraldehyde and 12 h for chitosan) [14,22]. As shown in Fig. S2, the obtained beads were repeatedly filtered and washed by water until the pH of beads was neutral. Finally, SA and CS beads were thus obtained and kept in pure water for further use.

The composite beads were prepared by the similar procedures as above mentioned. The difference was that the homogeneous aqueous solution is mixture of sodium alginate/chitosan and MIL-101(Cr) nanoparticles (mass ratio = 1:1).

2.3. Characterization

The presence of functional groups was confirmed by Fourier-transform infrared (FTIR) spectra recorded on a Bruker Tensor 27 IR spectrometer system using samples pelletized with KBr. X-ray diffraction (XRD) patterns were collected using a Rigaku D/max 2500VL/PC X-ray diffractometer equipped with a Cu-Kα radiation source to confirm the adsorbents structure. The morphology and element distribution of the adsorbents were characterized by transmission electron microscopy (TEM, JEOL-2100F), and scanning electron microscopy (SEM, JSM-7600F) equipped with energy-dispersive spectroscopy (EDS). BET surface areas were determined using nitrogen adsorption and desorption isotherms measured using a gas adsorption instrument (Micromeritics ASAP 2050 system). X-ray photoelectron spectroscopy (XPS) measurements were carried out on a ULVAC PHI-5000 VersaProbe using Al Kα X-ray as the excitation source. Prior to the above measurement, the samples were vacuum-dried at 60 °C for 24 h. After ultrasonicated for 15 min, Zeta potential (ZP) of the wet fragments from the samples was measured on a Malvern Nano-Z Zetasizer.

2.4. Adsorption experiments

Stock solutions of benzoic acid, ibuprofen and ketoprofen were prepared in pure ethanol at a concentration of 2.5 g/L and stored in a refrigerator (<0 °C) until used. Adsorption experiments were conducted in a series of 150 mL conical flasks, with a known initial concentration of three PPCPs aqueous solution and a designed amount of adsorbent. Flasks were sealed and placed in a New Brunswick G-25 incubator shaker with a shaking speed of 140 rpm. Kinetics experiments were carried out to determine the time for equilibrium. The concentrations before and after adsorption were analyzed by UV–vis spectrophotometry. The determination wavelengths were 224, 222 and 258 nm for benzoic acid, ibuprofen and ketoprofen, respectively. Detection limits of three pharmaceuticals were all 2 mg/L. Adsorption data were collected in triplicate for the pH experiments and in duplicate for all other experiments. The adsorption capacity, q_e (mg/g), was calculated according to Eq. (1).

$$q_e = \frac{(C_0 - C_e)V}{m} \quad (1)$$

where C_0 and C_e (mg/L) are the initial and equilibrium contaminant concentrations in water, respectively; V (L) is the volume of solution; m (g) is the mass of dried adsorbents.

2.5. Regeneration

After adsorption under selected optimal conditions, MIL-101 (Cr)/CS beads was separated from liquid by filtration. Then, a known volume of predesigned desorption solution was used to desorb the three PPCPs from MIL-101(Cr)/CS. After desorption equilibrium was reached, MIL-101(Cr)/CS was separated again from liquid by filtration for further reuse. Triplicates were performed, and average value was reported.

3. Results and discussion

3.1. Characterization of adsorbents

As shown in Fig. 1, MIL-101(Cr) nanoparticles could be well dispersed in water (Fig. 1D), it could be fixed into sodium alginate and chitosan natural polymers gels, and reconstructed the composite

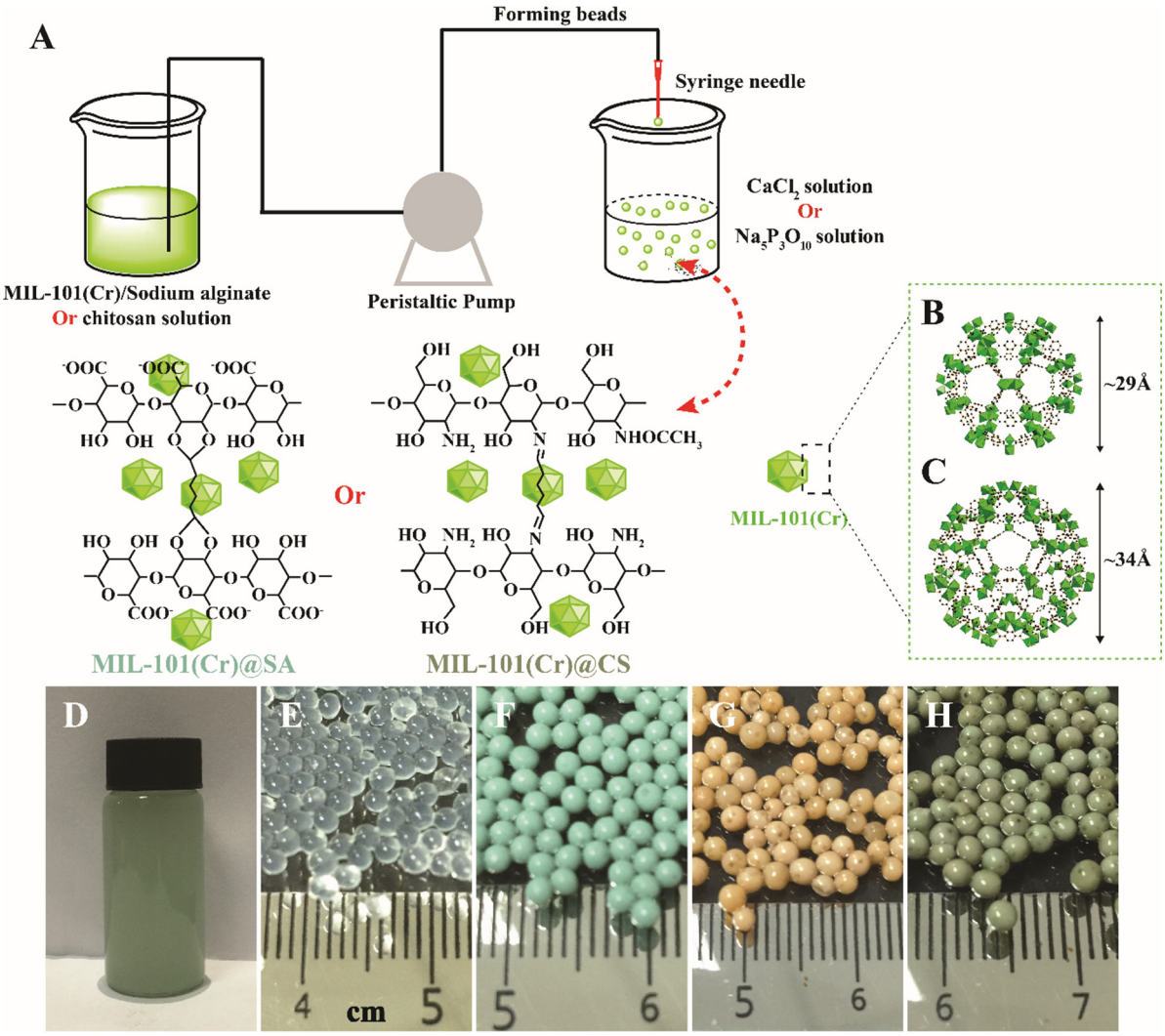

Fig. 1. Preparation procedures of the composite beads (A); the green dotted rectangle is the structures of MIL-101(Cr) – small cages (F) and large cages (G); the real pictures of MIL-101(Cr) nanoparticle solution (D), SA (E), MIL-101(Cr)/SA (F), CS (G) and MIL-101(Cr)@CS (H) beads. (For interpretation of the references to colour in this figure legend, the reader is referred to the web version of this article.)

beads (Fig. 1F and H). Comparing to pure SA and CS beads (Fig. 1E and G), MIL-101(Cr)/SA and MIL-101(Cr)/CS beads present greener due to the green MIL-101(Cr).

In Fig. 2A, the FTIR spectra of the raw MIL-101(Cr), sharp peaks with high intensity in the range of 1500–1650 cm^{-1} indicate the stretching vibrations of C=C bound of aromatic rings. Strong bands

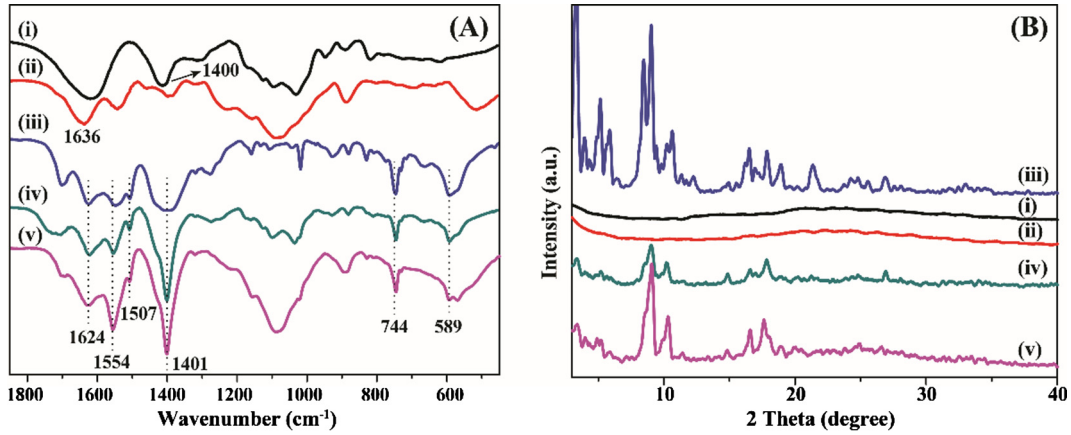

Fig. 2. Infrared spectra (A) and XRD patterns (B) obtained from the samples: SA (i, Black), CS (ii, Red), MIL-101(Cr) (iii, Blue), MIL-101(Cr)/SA (iv, Green) and MIL-101(Cr)/CS (v, Pink). (For interpretation of the references to colour in this figure legend, the reader is referred to the web version of this article.)

at 1401 and 744 cm^{-1} correspond to —COO^- vibration and C—H vibration of aromatic rings, respectively [23]. The peak with medium strength in 589 cm^{-1} is due to Cr—O vibrations, which proves the formation of metal organic framework indeed [23]. Similarly, in the FTIR spectrum of MIL-101(Cr)/SA and MIL-101(Cr)/CS, the same functional groups above mentioned are found around the corresponding 1624, 1554, 1507, 1401, 744 and 589 cm^{-1}. Therefore, it is concluded that MIL-101(Cr) has been successfully incorporated to the composite beads.

In Fig. 2B, XRD patterns show good crystallinity except SA and CS. The main diffraction peaks of raw MIL-101(Cr) were at 2θ = 3.25, 5.10, 8.41, 9.02, 16.49 and 17.40°, and relative diffraction intensities of the prepared samples are found to be the same as the standard data for MIL-101(Cr) [23]. The diffraction patterns of MIL-101(Cr)/SA and MIL-101(Cr)/CS are almost similar to that observed for MIL-101(Cr), which indicates that the structure of MIL-101(Cr) was preserved well.

In Supporting Information Fig. S3, TEM micrographs further reveal the presence of sodium alginate and chitosan on the surface of MIL-101(Cr), certifying both MIL-101(Cr)/SA and MIL-101(Cr)/CS have polymers-nanocrystal coating structure. Besides, MIL-101(Cr) nanocrystals show irregular morphology with a size around 500 nm. SEM images prove that, unlike relatively regular structure in pure SA and CS beads, more porous and looser structure can be found in the composite beads, which is expected to be beneficial for the adsorption of PPCPs (Supporting Information Fig. S4). EDS analysis (Supporting Information Fig. S5) confirms the formation of Cr element on MIL-101(Cr)/SA and MIL-101(Cr)/CS after MIL-101(Cr) incorporated with sodium alginate and chitosan. EDX elemental mappings indicate that MIL-101(Cr) nanoparticles distributed uniformly in the composite beads.

In Supporting Information Fig. S6, nitrogen adsorption-desorption measurements were carried out to determine the specific surface areas of raw MIL-101(Cr) and four adsorbents. The BET surface areas of MIL-101(Cr)/SA and MIL-101(Cr)/CS are much higher than those of pristine SA and CS, from 1.5 to 720 m^2/g and from 48 to 800 m^2/g respectively, indicating that the ordered nanopore-structure of MIL-101(Cr) in the composite beads is preserved well [24].

3.2. Adsorption kinetics

Fig. 3 compares the three PPCPs adsorption kinetics onto the four adsorbents at their initial pH without adjustment. All adsorption amounts of adsorbents follow the order of MIL-101(Cr)/CS > MIL-101(Cr)/SA > CS > SA to three PPCPs (BET, IBU, and KET), suggesting that the presence of MIL-101(Cr) plays a significant role in improving the interactions between the adsorbates and the composite beads.

In general, adsorption amounts onto the composite beads increase quickly in the first 60 min of contact time with about 70–80% equilibria adsorption amounts and then achieve the adsorption equilibrium after ~180 min. The greater adsorption amounts and higher adsorption rates indicate that MIL-101(Cr)/CS beads possess the competitive advantage for the PPCPs removal.

To evaluate the kinetic adsorption mechanism, three adsorption kinetics models, namely the pseudo-first-order, the pseudo-second-order, and the intra-particle diffusion models were selected to fit the dynamic data. Detailed description on kinetic models is provided in Supporting Information Text S2. The data in Supporting Information Table S2 show that pseudo-second-order kinetic model (R^2 > 0.98) could fit the adsorption data well onto the CS, MIL-101(Cr)/SA and MIL-101(Cr)/CS. As is known, the pseudo-second-order model is commonly related to the chemical adsorption process and the number of active sites on the sorbent determines the adsorption capacity [25]. The high

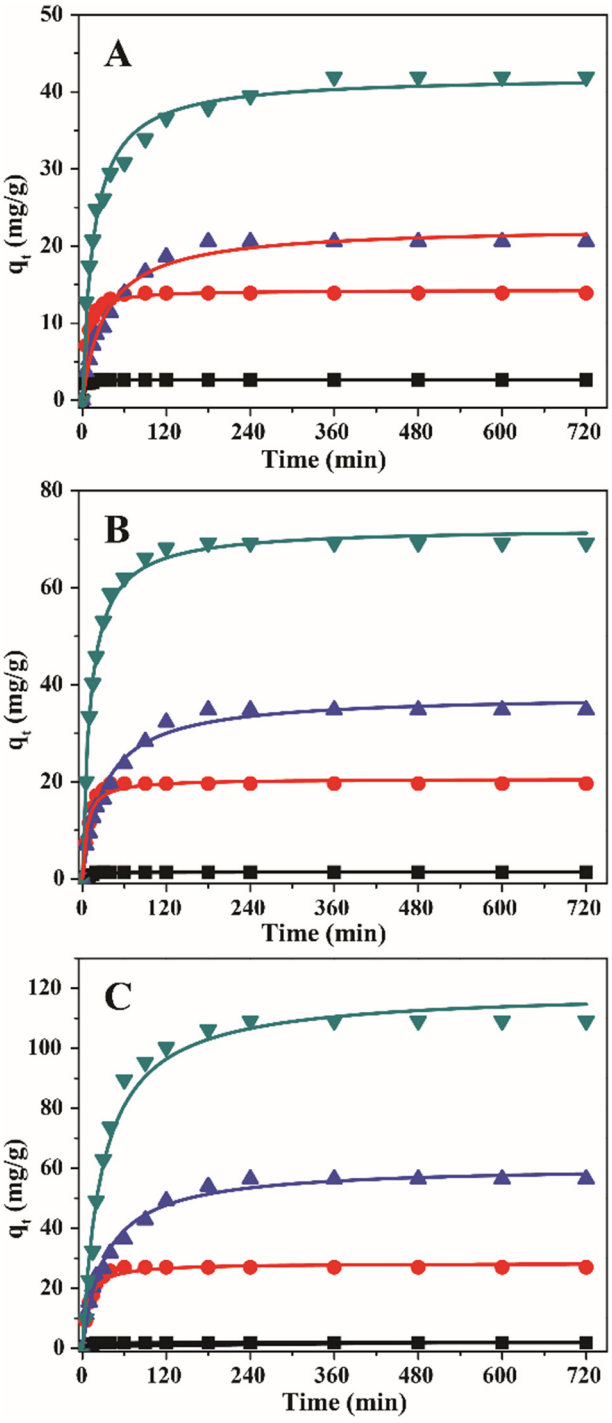

Fig. 3. Adsorption kinetics of BEN (A), IBU (B), and KET (C) onto SA (■, Black), CS (●, Red), MIL-101(Cr)/SA (▲, Blue) and MIL-101(Cr)/CS (▼, Green) at initial pH. The soild lines are the curve fitting using pseudosecond-order model (For interpretation of the references to colour in this figure legend, the reader is referred to the web version of this article.).

correlation coefficients (R^2) imply there possibly exist chemical interactions between PPCPs and the adsorbents. Given that the three PPCPs partially exist in their anionic forms at initial pH of 4.08, 4.27, and 4.23 respectively, the protonated amine cationic sites on the CS can capture three PPCPs anion by electrostatic attraction [18]. Meantime, the surface of raw MIL-101(Cr) nanoparticles are positively charged in the pH = 4–5 range [8], indicating that the electrostatic interaction may dominate the

adsorption of three PPCPs on the composite beads. It is in agreement with the fact of the fast kinetics. Besides, it is found that contaminants with higher molecular weight possess higher adsorption amounts [26].

3.3. Effect of pH

The pH was one of the most important parameter influencing the adsorption as it will change both the surface chemical properties of adsorbent and the solution chemistry of adsorbate in aqueous solution. Fig. 4 shows the effects of pH on the adsorption of the three PPCPs. The result indicates that, during the adsorption process, the solution pH has obvious influences on the adsorption. To better understand the effect of the pH-dependent surface charge, the zeta potential of raw MIL-101(Cr) and the four adsorbents were explored and presented in Fig. 5.

As depicted in Fig. 5, CS beads are positively charged when the pH is lower than 7.5, which could attract the PPCPs anions; on the other hand, the surface charge of SA was mostly negatively charged in the tested pH range, resulting in little or no uptake of the PPCPs. The surface of raw MIL-101(Cr) is mostly positively charged in the pH = 2–8 range, similar trend of ZP-pH curve has been observed by Liu et al. [8], and they also have proposed that the raw MIL-101(Cr) can effectively adsorb anionic organic pollutants by electrostatic attraction. The ZPs of MIL-101(Cr)/SA and MIL-101/(CS) demonstrate that the composite beads possess higher ZPs than pristine SA and CS beads at different pH, respectively, which should be ascribed to the presence of MIL-101(Cr). Thus, the enhanced adsorption amounts of the PPCPs can be partly resulted from the electrostatic interaction between the PPCPs and the composite beads. However, electrostatic attraction is not the only interaction between contaminants and the adsorbents, since it is found that MIL-101(Cr)/SA beads with more negative ZP exert better performance than CS beads. Other interactions are therefore deduced to exist, which will be discussed in following sections.

Furthermore, the adsorption amounts of three PPCPs onto MIL-101(Cr)/SA are lower than those of MIL-101(Cr)/CS, which is related to the different surface charge of sodium alginate (negative) and chitosan (positive) on the composite beads. Meanwhile, for a given adsorbent, three PPCPs adsorbed onto the CS, MIL-101 (Cr)/SA and MIL-101(Cr)/CS exhibit similar patterns of pH-dependence, suggesting again the predominant influence of electrostatic attraction in adsorption. The pH-dependent effects are correlated with the pH-regulated distribution of the various species of three PPCPs. It is in agreement with previous studies that the obvious transformation of adsorbed amounts can be observed at their initial pH values [27]. On the other hand, for a given adsorbate, the three adsorbents exhibit a little different pH-dependent patterns, suggesting that pH effects are somewhat adsorbent-specific.

Moreover, CS beads have little or no adsorption amounts when it is in the main existence of neutral molecule form or at pH higher

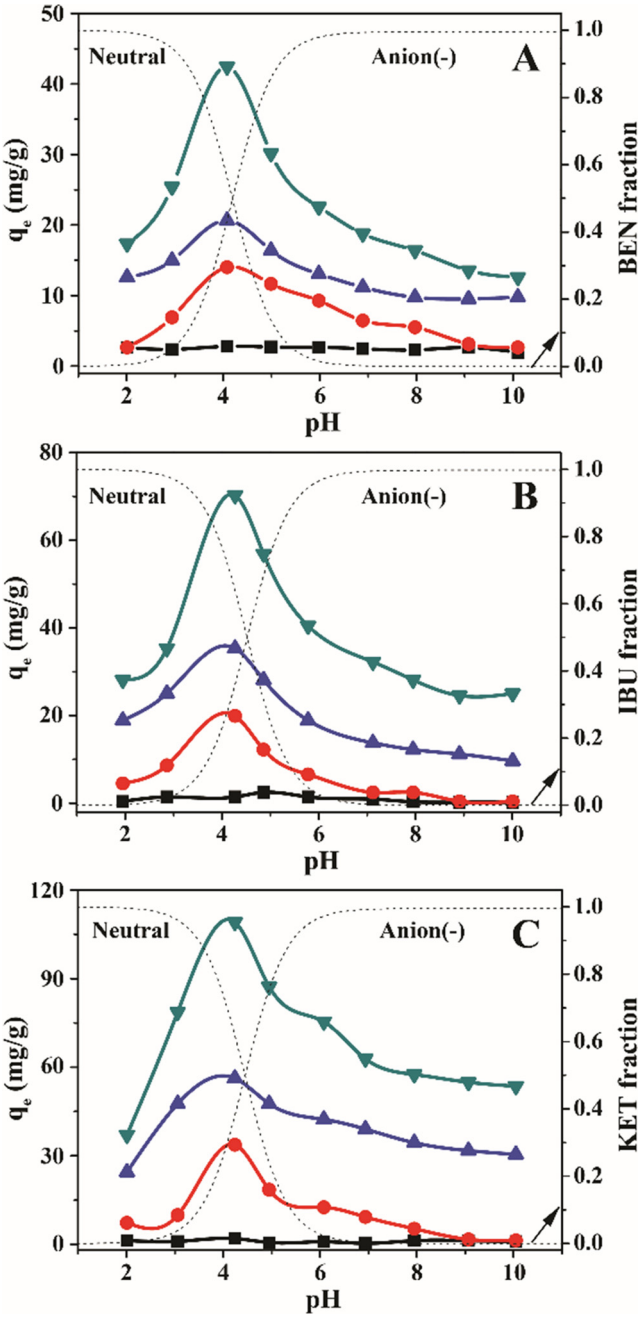

Fig. 4. Adsorption of BEN (A), IBU (B), and KET (C) onto SA (■, Black), CS (●, Red), MIL-101(Cr)/SA (▲, Blue) and MIL-101(Cr)/CS (▼, Green) at varying pH. The dashed lines represent the fractions of neutral and anionic forms of the adsorbates. (For interpretation of the references to colour in this figure legend, the reader is referred to the web version of this article.)

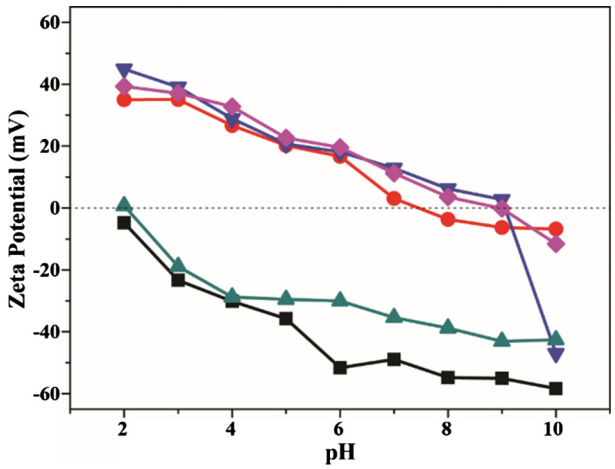

Fig. 5. Zeta potentials of SA (■, Black), CS (●, Red), MIL-101(Cr)/SA (▲, Green), MIL-101(Cr)/CS (▼, Blue) and raw MIL-101(Cr) (◆, Brown) at varying pH. (For interpretation of the references to colour in this figure legend, the reader is referred to the web version of this article.)

than its isoelectric point. Instead, MIL-101(Cr)/SA and MIL-101(Cr)/CS still can remove the PPCPs under the above conditions, indicating that other non-electrostatic mechanisms, in addition to charge attraction, are possible to exist as follows: (i) The ordered nanopores providing inner diffusion for the adsorbates molecular; (ii) π-π interactions between π-electrons of MIL-101(Cr) nanocrystal and the adsorbates aromatic rings.

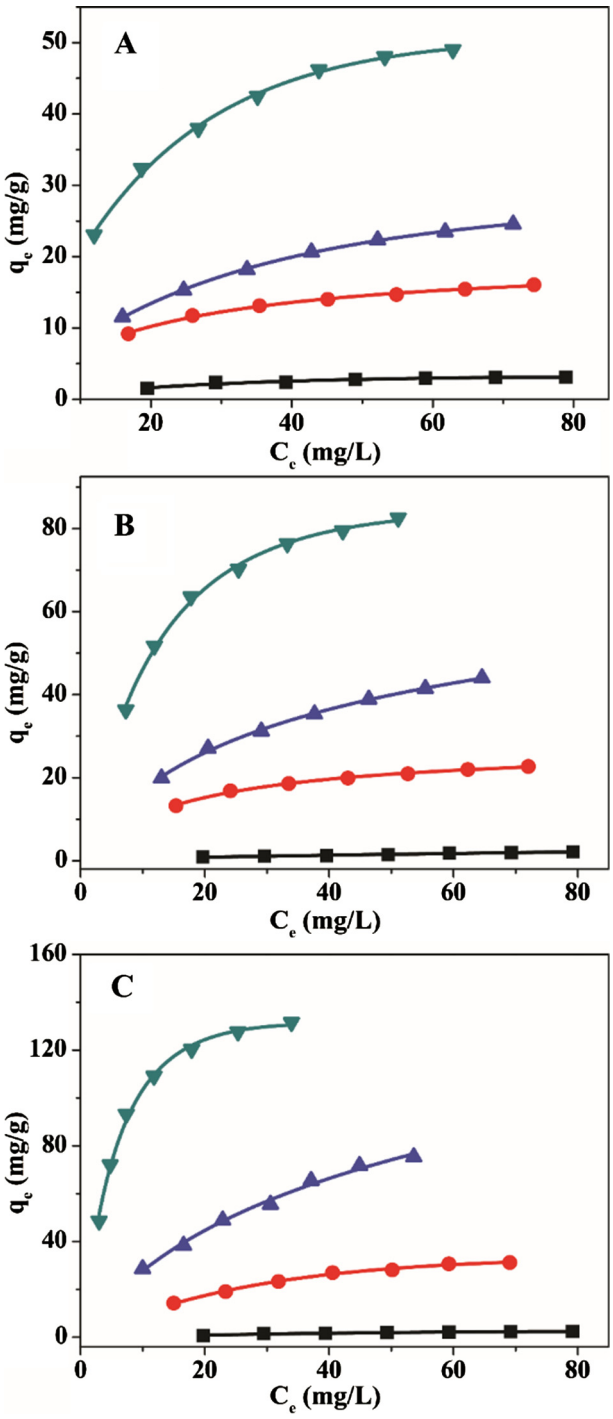

Fig. 6. Adsorption isotherms of BEN (A), IBU (B), and KET (C) onto SA (■, Black), CS (●, Red), MIL-101(Cr)/SA (▲, Blue) and MIL-101(Cr)/CS (▼, Green) at initial pH. The soild lines are the curve fitting using Redlich-Perterson model. (For interpretation of the references to colour in this figure legend, the reader is referred to the web version of this article.)

3.4. Adsorption isotherms

Adsorption isotherms of the three PPCPs onto the four adsorbents were depicted in Fig. 6. Three models of Langmuir, Freundlich and Redlich-Perterson in Supporting Information Text S3 are selected to fit the experimental data and the results are listed in Supporting Information Table S3. The Freundlich isotherm is an empirical equation employed to describe heterogeneous systems while the Langmuir adsorption isotherm assumes a homogeneous adsorption process. The Redlich-Peterson isotherm model combines elements from both the Langmuir and Freundlich equations, and the mechanism of adsorption is a hybrid one and does not follow ideal monolayer adsorption. As shown in Supporting Information Table S3, the high correlation coefficients ($R^2 > 0.99$) of adsorption isotherms except SA adsorption isotherms certify that the Redlich-Peterson model can better describe adsorption isotherms. This suggests that the adsorption processes might be hybrid processes. Simultaneously, the adsorption isotherms on CS could be better fitted by Langmuir model ($R^2 > 0.99$) due to the dominant electrostatic attraction.

To thoroughly understand the hybrid processes, the unit of the adsorption amounts were converted to mmol/g and some interesting changes took place among the adsorption of three PPCPs. As shown in Supporting Information Fig. S7, the adsorption amounts of three PPCPs onto CS are approximately equal, possibly due to the definite adsorption sites of electrostatic interaction [26]. However, the adsorption amounts of KET onto MIL-101(Cr)/SA and MIL-101(Cr)/CS are obviously greater than those of IBU and BEN, suggesting the difference of KET molecular structure compared to BEN and IBU molecule: KET molecule possesses more than one benzene ring, which can effectively enhance its π-energy.

π-energy is calculated by the Hückel molecular orbital (HMO) method, which is a theory for determining molecular structure in which electrons are not assigned to individual bonds between atoms, but are treated as moving under the influence of the nuclei in the whole molecule [28]. As shown in Supporting Information Table S1, π-energy of three PPCPs follows the order of KET (27.87) > IBU(15.7) ≈ BEN(16.13), determining that the π electrons of KET have the larger energy of molecular orbitals. Therefore, the adsorption of KET onto MIL-101(Cr)/CS can enhance π-π interaction between π-electrons of the adsorbents and the KET molecules with the richer π electrons [29,30], further leading to the greater adsorption amounts (mmol/g).

3.5. Adsorption mechanism

XPS analysis of MIL-101(Cr)/CS composite beads before and after the adsorption of three PPCPs were carried out to further investigate the interactions between the three PPCPs and MIL-101(Cr)/CS. As shown in Fig. 7, the N1s spectrum of MIL-101(Cr)/CS (Fig. 7A) is dissected into three peaks at binding energies of 399.5, 400.5 and 401.7 eV, corresponding to the nitrogen in the amine (1: —$\underline{N}H_2$), amide (2: —$\underline{N}H$—C=O), and protonated amine (3: —$\underline{N}H_3^+$), respectively [31]. After adsorption, all peaks at 401.7 eV rise markedly in Fig. 7B –D, which could be assigned to the more protonated amine coordinated with the PPCPs [32]. These features demonstrate that the amine groups participate in the adsorption of PPCPs through electrostatic interaction. The peaks of 586.4 and 576.8 eV are attributed to Cr $2p_{1/2}$ and Cr $2p_{3/2}$, respectively (Fig. 7E) [33,34]. After the adsorption of PPCPs, all peaks of Cr $2p_{1/2}$ shifted from 586.4 (virgin adsorbent) to 585.9 eV, and the peak of Cr $2p_{3/2}$ slightly shifted down by 0.5 to 576.2 eV. The decrease of the binding energy of chromium should be ascribed to the formation of Cr—O bonds between Cr atoms and

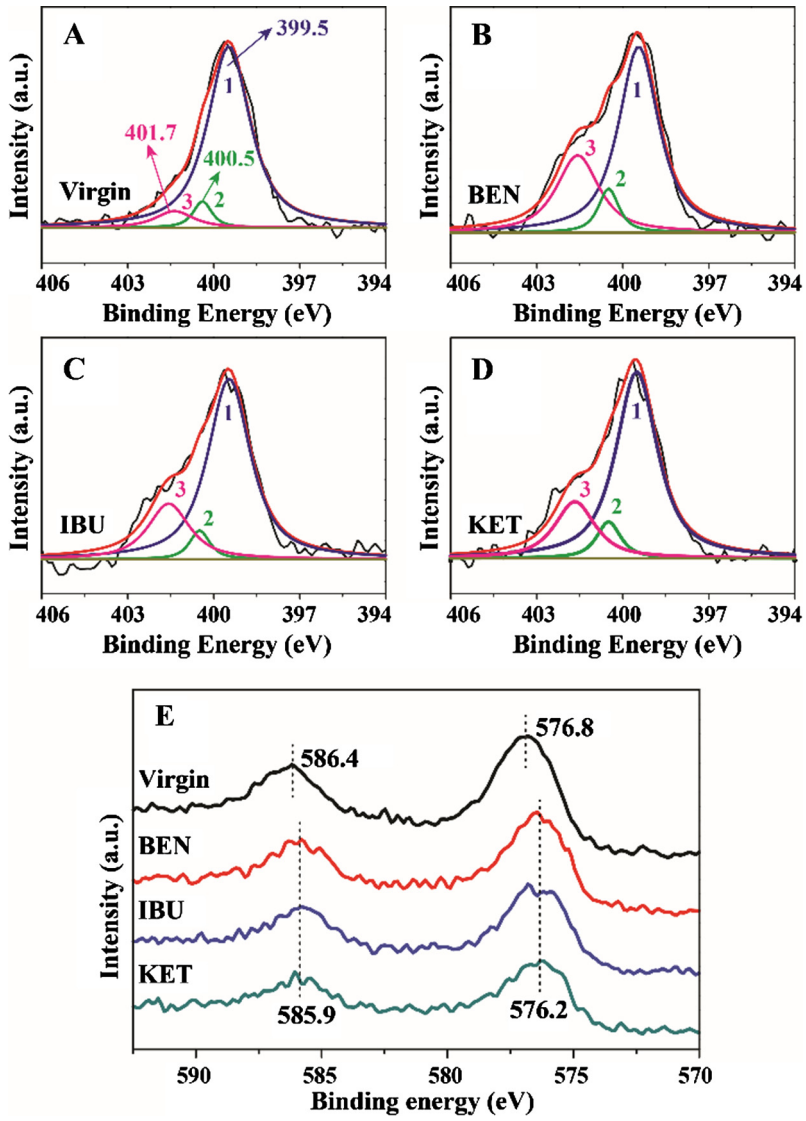

Fig. 7. N 1s (A, B, C, D), Cr 2p (E) XPS spectra of MIL-101(Cr)/CS (virgin) and MIL-101(Cr)/CS with BEN, IBU and KET species adsorbed (BEN, IBU and KET).

the carboxylic groups of PPCPs. The XPS analysis indicates that the amine on the chitosan matrix and Cr center on the MIL-101(Cr) both participate in adsorbing the PPCPs.

Therefore, on the basis of above investigation, it is proposed that the adsorption of PPCPs on MIL-101(Cr)/CS composite bead was mainly controlled by the electrostatic attraction and π-π interaction and the suggested mechanisms are schematically summarized in Fig. 8.

3.6. Effect of ionic strength and reusability

The effects of ionic strength on the adsorption of three PPCPs were presented in Supporting Information Fig. S8. The decreased adsorption of PPCPs onto the adsorbents are observed with the increasing NaCl concentration, indicating that chloride anions could compete with the PPCPs anions for the same adsorption sites on the adsorbents. The three PPCPs adsorption onto MIL-101(Cr)/SA and MIL-101(Cr)/CS also decreased at lower ionic concentration due to chloride anions competition, while the adsorption amounts are almost unchanged with the ionic concentration of >0.25 wt.%, also suggesting that both electrostatic attraction and π-π interaction make contributions to the adsorption.

The reusability of the adsorbent is considered to be one of the most important criteria to evaluate the feasibility of engineering application. With the above observation that MIL-101(Cr)/CS exhibits slightly reduced adsorption amounts by the influence of co-existing ions and the three PPCPs freely dissolves in ethanol, 0.2 wt.% NaCl/ethanol-water (volume ratio = 3:7) solution was chosen as the desorption agent for the regeneration study. As shown in Fig. 9A, the adsorption-desorption cycles were repeated seven times. Compared to the virgin MIL-101(Cr) nanoparticle, the regenerated beads present excellent reusability and consistency with about 5% decrease in the adsorption amounts after seven cycles. XRD patterns (Fig. 9B) clearly shows MIL-101(Cr)/CS beads still show good crystallinity at seventh adsorption cycles. This suggests the attached MIL-101(Cr) moiety could keep stable during repeated regeneration process. Therefore, the excellent reusability of MIL-101(Cr)/CS composite beads demonstrates its great possibility in long-term large scale water treatment, such as advanced wastewater treatment, and household drinking water purification systems.

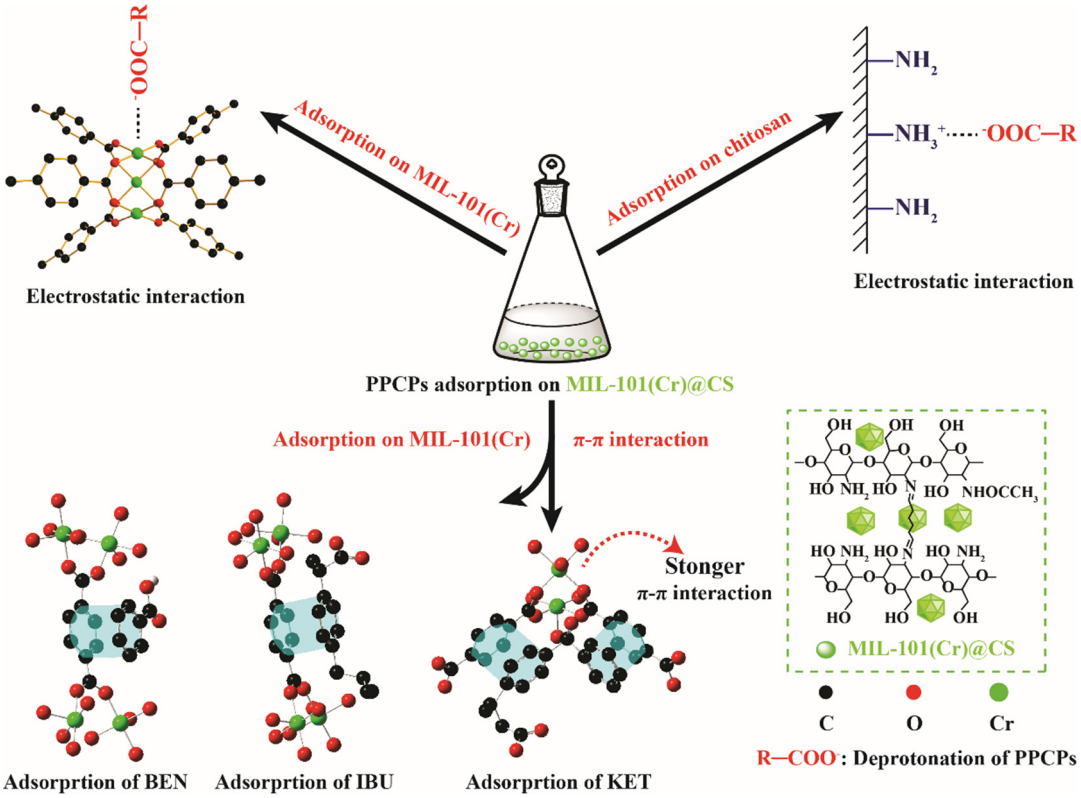

Fig. 8. Mechanistic illustration of adsorption of three PPCPs on MIL-101(Cr)/CS.

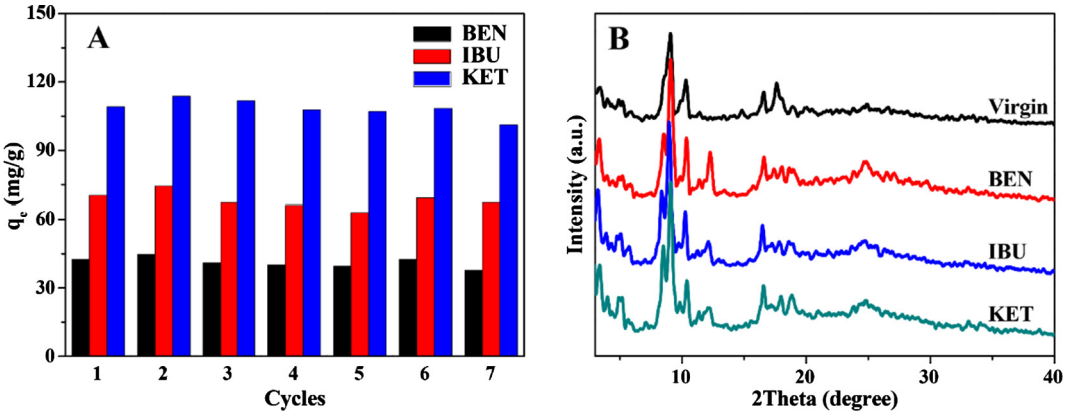

Fig. 9. A: Recycling of MIL-101(Cr)/CS in the adsorption of BEN, IBU and KET; B: XRD patterns of MIL-101(Cr)/CS after seven cycles adsorption-desorption.

4. Conclusion

We report the synthesis of composite beads MIL-101(Cr)/CS and MIL-101(Cr)/SA via a two-step method. The as-synthesized MIL-101(Cr)/SA and MIL-101(Cr)/CS composite beads have rough surface and average diameter of 2–3 mm, respectively. Batch adsorption experiments reveal that MIL-101(Cr)/CS beads are more effective in removing PPCPs. The underlying mechanism of three PPCPs adsorption is investigated by the kinetics, pH effect, isotherms, π-energy calculation and instrumental analysis. The protonated amine groups and the Cr center of the adsorbents wield electrostatic interactions with the deprotonated carboxyl groups of the contaminants, and stronger π-π interaction of aromatic rings between MIL-101(Cr) and the adsorbates with larger π-energy also contributes to the adsorption. The present work suggests that MIL-101(Cr)/CS beads, owing to their easy separation, rapid adsorption rate and high capacities and good regenerability, have great potential as the excellent adsorbent in the removal of PPCPs and other emerging contaminants.

Acknowledgments

This study was supported by the National Natural Science Foundation of China (51608275), the Natural Science Foundation of Jiangsu Province of China (BK20161480, BK20150981), the Natural Science Foundation of the Jiangsu Higher Education Institutions of China (15KJB610009), and the Priming Scientific Research Foundation for Advanced Talents of Nanjing Normal University (2014103XGQ0196). We also appreciate the Foundation of Jiangsu Collaborative Innovation Center of Biomedical Functional Materials, and a project funded by the Priority Academic Program Development of Jiangsu Higher Education Institutions.

Appendix A. Supplementary data

Supplementary data associated with this article can be found, in the online version, at http://dx.doi.org/10.1016/j.seppur.2016.12.041.

References

[1] S.D. Richardson, T.A. Ternes, Water analysis: emerging contaminants and current issues, Anal. Chem. 86 (2014) 2813–2848.
[2] P. Westerhoff, Y. Yoon, S. Snyder, E. Wert, Fate of endocrine-disruptor, pharmaceutical, and personal care product chemicals during simulated drinking water treatment processes, Environ. Sci. Technol. 39 (2005) 6649–6663.
[3] W.-K. Jo, T.S. Natarajan, Facile synthesis of novel redox-mediator-free direct Z-scheme $CaIn_2S_4$ marigold-flower-like/TiO_2 photocatalysts with superior photocatalytic efficiency, ACS Appl. Mater. Interfaces 7 (2015) 17138–17154.
[4] M. Grassi, L. Rizzo, A. Farina, Endocrine disruptors compounds, pharmaceuticals and personal care products in urban wastewater: implications for agricultural reuse and their removal by adsorption process, Environ. Sci. Pollut. Res. Int. 20 (2013) 3616–3628.
[5] S. Shanmuganathan, T.V. Nguyen, S. Jeong, J. Kandasamy, S. Vigneswaran, Submerged membrane-(GAC) adsorption hybrid system in reverse osmosis concentrate treatment, Sep. Purif. Technol. 146 (2015) 8–14.
[6] M. Grassi, L. Rizzo, A. Farina, Endocrine disruptors compounds, pharmaceuticals and personal care products in urban wastewater: implications for agricultural reuse and their removal by adsorption process, Environ. Sci. Pollut. Res. Int. 20 (2013) 3616–3628.
[7] L. Ji, F. Liu, Z. Xu, S. Zheng, D. Zhu, Adsorption of pharmaceutical antibiotics on template-synthesized ordered micro- and mesoporous carbons, Environ. Sci. Technol. 44 (2010) 3116–3122.
[8] K. Liu, S. Zhang, X. Hu, K. Zhang, A. Roy, G. Yu, Understanding the adsorption of PFOA on MIL-101(Cr)-based anionic-exchange metal-organic frameworks: comparing DFT calculations with aqueous sorption experiments, Environ. Sci. Technol. 49 (2015) 8657–8665.
[9] H.-P. Jing, C.-C. Wang, Y.-W. Zhang, P. Wang, R. Li, Photocatalytic degradation of methylene blue in ZIF-8, RSC Adv. 4 (2014) 54454–54462.
[10] E. Haque, V. Lo, A.I. Minett, A.T. Harris, T.L. Church, Dichotomous adsorption behaviour of dyes on an amino-functionalised metal–organic framework, amino-MIL-101(Al), J. Mater. Chem. A 2 (2014) 193–203.
[11] J.W. Jun, M. Tong, B.K. Jung, Z. Hasan, C. Zhong, S.H. Jhung, Effect of central metal ions of analogous metal-organic frameworks on adsorption of organoarsenic compounds from water: plausible mechanism of adsorption and water purification, Chemistry 21 (2015) 347–354.
[12] B. Liu, F. Yang, Y. Zou, Y. Peng, Adsorption of phenol and p-nitrophenol from aqueous solutions on metal-organic frameworks: effect of hydrogen bonding, J. Chem. Eng. Data 59 (2014) 1476–1482.
[13] L. Huang, M. He, B. Chen, B. Hu, A designable magnetic MOF composite and facile coordination-based post-synthetic strategy for the enhanced removal of Hg^{2+} from water, J. Mater. Chem. A 3 (2015) 11587–11595.
[14] Y. Zhen, Z. Ning, Z. Shaopeng, D. Yayi, Z. Xuntong, S. Jiachun, Y. Weiben, W. Yuping, C. Jianqiang, A pH- and temperature-responsive magnetic composite adsorbent for targeted removal of nonylphenol, ACS Appl. Mater. Interfaces 7 (2015) 24446–24457.
[15] A. Ouyang, C. Wang, S. Wu, E. Shi, W. Zhao, A. Cao, D. Wu, Highly porous core-shell structured graphene-chitosan beads, ACS Appl. Mater. Interfaces 7 (2015) 14439–14445.
[16] K.Z. Elwakeel, A.A. Atia, E. Guibal, Fast removal of uranium from aqueous solutions using tetraethylenepentamine modified magnetic chitosan resin, Bioresour. Technol. 160 (2014) 107–114.
[17] N. Wu, H. Wei, L. Zhang, Efficient removal of heavy metal ions with biopolymer template synthesized mesoporous titania beads of hundreds of micrometers size, Environ. Sci. Technol. 46 (2012) 419–425.
[18] Y.T. Wei, Y.M. Zheng, J.P. Chen, Design and fabrication of an innovative and environmental friendly adsorbent for boron removal, Water Res. 45 (2011) 2297–2305.
[19] H. Demey, T. Vincent, M. Ruiz, M. Nogueras, A.M. Sastre, E. Guibal, Boron recovery from seawater with a new low-cost adsorbent material, Chem. Eng. J. 254 (2014) 463–471.
[20] G. Ferey, C. Mellot-Draznieks, C. Serre, F. Millange, J. Dutour, S. Surble, I. Margiolaki, A chromium terephthalate-based solid with unusually large pore volumes and surface area, Science 309 (2005) 2040–2042.
[21] Y. Huang, Y. Lapitsky, Monovalent salt enhances colloidal stability during the formation of chitosan/tripolyphosphate microgels, Langmuir 27 (2011) 10392–10399.
[22] A.W. Chan, R.A. Whitney, R.J. Neufeld, Kinetic controlled synthesis of pH-responsive network alginate, Biomacromolecules 9 (2008) 2536–2545.
[23] R. Fazaeli, H. Aliyan, M. Moghadam, M. Masoudinia, Nano-rod catalysts: building MOF bottles (MIL-101 family as heterogeneous single-site catalysts) around vanadium oxide ships, J. Mol. Catal. A – Chem. 374–375 (2013) 46–52.
[24] M. Wickenheisser, A. Herbst, R. Tannert, B. Milow, C. Janiak, Hierarchical MOF-xerogel monolith composites from embedding MIL-100(Fe, Cr) and MIL-101 (Cr) in resorcinol-formaldehyde xerogels for water adsorption applications, Micropor. Mesopor. Mat. 215 (2015) 143–153.
[25] H. Li, C. Shan, Y. Zhang, J. Cai, W. Zhang, B.C. Pan, Arsenate adsorption by hydrous ferric oxide nanoparticles embedded in cross-linked anion exchanger: effect of the host pore structure, ACS Appl. Mater. Interfaces 8 (2016) 3012–3020.
[26] W.T. Tsai, C.Y. Chang, C.H. Ing, C.F. Chang, Adsorption of acid dyes from aqueous solution on activated bleaching earth, J. Colloid Interf. Sci. 275 (2004) 72–78.
[27] Z. Hasan, E.-J. Choi, S.H. Jhung, Adsorption of naproxen and clofibric acid over a metal–organic framework MIL-101 functionalized with acidic and basic groups, Chem. Eng. J. 219 (2013) 537–544.
[28] K. Cocq, C. Lepetit, V. Maraval, R. Chauvin, "Carbo-aromaticity" and novel carbo-aromatic compounds, Chem. Soc. Rev. 44 (2015) 6535–6559.
[29] D.Q. Zhu, J.J. Pignatello, Characterization of aromatic compound sorptive interactions with black carbon (charcoal) assisted by graphite as a model, Environ. Sci. Technol. 39 (2005) 2033–2041.
[30] F. Xiao, J.J. Pignatello, Pi(+)-pi interactions between (hetero)aromatic amine cations and the graphitic surfaces of pyrogenic carbonaceous materials, Environ. Sci. Technol. 49 (2015) 906–914.
[31] D. Wan, S. Yuan, G.L. Li, K.G. Neoh, E.T. Kang, Glucose biosensor from covalent immobilization of chitosan-coupled carbon nanotubes on polyaniline-modified gold electrode, ACS Appl. Mater. Interfaces 2 (2010) 3083–3091.
[32] T. Chen, F. Liu, C. Ling, J. Gao, C. Xu, L. Li, A. Li, Insight into highly efficient coremoval of copper and p-nitrophenol by a newly synthesized polyamine chelating resin from aqueous media: competition and enhancement effect upon site recognition, Environ. Sci. Technol. 47 (2013) 13652–13660.
[33] M.-G. Jeong, D.H. Kim, S.-K. Lee, J.H. Lee, S.W. Han, E.J. Park, K.A. Cychosz, M. Thommes, Y.K. Hwang, J.-S. Chang, Y.D. Kim, Decoration of the internal structure of mesoporous chromium terephthalate MIL-101 with NiO using atomic layer deposition, Micropor. Mesopor. Mat. 221 (2016) 101–107.
[34] T.A. Vu, G.H. Le, C.D. Dao, L.Q. Dang, K.T. Nguyen, P.T. Dang, H.T.K. Tran, Q.T. Duong, T.V. Nguyen, G.D. Lee, Isomorphous substitution of Cr by Fe in MIL-101 framework and its application as a novel heterogeneous photo-Fenton catalyst for reactive dye degradation, RSC Adv. 4 (2014) 41185–41194.